catalysts

MDPI

Article

Effect of Water Molecule on Photo-Assisted Nitrous Oxide Decomposition over Oxotitanium Porphyrin: A Theoretical Study

Phornphimon Maitarad [1,2,*], Vinich Promarak [2,3], Liyi Shi [1] and Supawadee Namuangruk [1,4,*]

1 Research Center of Nano Science and Technology, Shanghai University, Shanghai 200444, China; shiliyi@shu.edu.cn
2 Department of Materials Science and Engineering, School of Molecular Science and Engineering, Vidyasirimedhi Institute of Science and Technology, Rayong 21210, Thailand; vinich.p@vistec.ac.th
3 Research Network of NANOTEC-VISTEC on Nanotechnology for Energy, Vidyasirimedhi Institute of Science and Technology, Wangchan, Rayong 21210, Thailand
4 National Nanotechnology Center (NANOTEC), NSTDA, 111 Thailand Science Park, Pahonyothin Road, Klong Luang, Pathum Thani 12120, Thailand
* Correspondence: pmaitarad@shu.edu.cn (P.M.); supawadee@nanotec.or.th (S.N.)

Received: 3 January 2020; Accepted: 21 January 2020; Published: 1 February 2020

check for updates

Abstract: Water vapor has generally been recognized as an inhibitor of catalysts in nitrous oxide (N_2O) decomposition because it limits the lifetime of catalytic reactors. Oxygen produced in reactions also deactivates the catalytic performance of bulk surface catalysts. Herein, we propose a potential catalyst that is tolerant of water and oxygen in the process of N_2O decomposition. By applying density functional theory calculations, we investigated the reaction mechanism of N_2O decomposition into N_2 and O_2 catalyzed by oxotitanium(IV) porphyrin (TiO-por) with interfacially bonded water. The activation energies of reaction Path A and B are compared under thermal and photo-assisted conditions. The obtained calculation results show that the photo-assisted reaction in Path B is highly exothermic and proceeds smoothly with the low activation barrier of 27.57 kcal/mol at the rate determining step. The produced O_2 is easily desorbed from the surface of the catalyst, requiring only 4.96 kcal/mol, indicating the suppression of catalyst deactivation. Therefore, TiO-por is theoretically proved to have the potential to be a desirable catalyst for N_2O decomposition with photo-irradiation because of its low activation barrier, water resistance, and ease of regeneration.

Keywords: metal-porphyrin; N_2O decomposition; reaction mechanism; catalysis; density functional theory

1. Introduction

Nitrous oxide (N_2O) is an anthropogenic gas reported as the largest contribution to the ozone depleting gas emissions [1]. Once it is transported to the stratosphere, it destroys the ozone and causes the greenhouse effect. At present, the development of technologies for the abatement of N_2O mainly focuses on (i) nonselective catalytic reduction, (ii) selective catalytic reduction, and (iii) direct catalytic decomposition. Among the up-to-date technologies, the direct decomposition of N_2O (*de*N_2O) has attracted much attention because of its efficiency and cost effectiveness [2–5]. Researches in the field of N_2O catalytic decomposition mainly focus on low-temperature *de*N_2O catalysts that can be applied to N_2O abatement in medical operating rooms, nitric acid plants, three-way catalytic converters, etc. For example, N_2O is used as an anesthetic gas in hospitals and it can lead to miscarriages in gestation, liver disorder, kidney trouble, and so on. Doi et al. [6,7] worked on the *de*N_2O of the air contaminated with N_2O in operating rooms by varying the alumina-supported metals (Pt, Pd, or Rh), and found that the Rh/Al_2O_3 is the most suitable catalyst for *de*N_2O in operating rooms which could reach 100% decomposition at 773K.

The catalytic *de*N_2O has been studied to a greater extent than selective catalytic reduction (SCR) over a large variety of catalysts, including noble metals [4,8–11], perovskites [12–14], metal oxides [15–18], and zeolites [19–22]. It is also important to note that in *de*N_2O processes, tolerance to various substances coexisting in the exhaust gases (e.g. NO_x, SO_2, O_2, and H_2O) should be simultaneously accomplished without sacrificing low-temperature activity. For example, the effect of SO_2 and/or H_2O on the NO_x and N_2O reduction was examined over the In/Al_2O_3-Ru/Al_2O_3 dual-bed reactor. Their transient experiments showed that the N_2O conversion dropped to zero in the presence of SO_2 and H_2O [23,24]. In addition, there have been reports of various catalysts which show that their catalytic performance of *de*N_2O is decreased due to the active site poisoned with water vapor or oxygen molecules produced during the reaction [25–28]. Regarding to water inhibition, it was studied, theoretically, by Heyden et al. [27] who concluded that water impurity (<100 ppm) may strongly affect the kinetics of N_2O decomposition, leading to an increase in apparent activation energy for 26 kcal/mol approximately. It is, obviously, important to take into account both the reaction mechanism and activation energy. In addition, those who are working on development of new catalysts for *de*N_2O should consider the effect of water at the active sites as well as the catalytic site regeneration by oxygen desorption, which is key to the reaction.

Besides thermal *de*N_2O, photo-assisted direct decomposition is another alternative method for N_2O removal [29–31]. This method applies light as the energy source for initiating the reaction, and the catalysis is active even at low gas concentration and low temperature. Therefore, with a suitable catalyst, a photocatalytic under the UV and near UV lights with wavelength 200–400 nm can be applied to decompose N_2O. In general, N_2O is decomposed into N_2 and O_2 under a photocatalytic reaction [32] by

$$N_2O \overset{hv,\ catalyst}{\rightarrow} N_2 + \frac{1}{2}\,O_2 \tag{1}$$

The well-accepted photo-catalyst for N_2O decomposition is TiO_2 loaded with various noble metals [33–36]. However, noble metals are expensive for practical uses. Thus, a search for low-cost and effective catalysts for photocatalytic N_2O decomposition has been of great interest.

Porphyrin is a potential compound because it possesses two axial coordination sites which are suitable for anchoring to a solid substrate, such as in the metal-porphyrin assembly that features in several useful applications, including photovoltaic materials, field-responsive materials, and catalytic materials [37–40]. In our previous theoretical work [41], we proposed that low-valent titanium(II)-porphyrin (Ti-por) is a good catalyst for *de*N_2O under thermal conditions; the activation energies in the energy profiles are comparable to other potential catalysts. However, this low-valent Ti-por can be easily oxidized to form a more stable structure, reducing its suitability. The high-valent oxotitanium(IV)-porphyrin (TiO-por) is a better choice and has been reported as a potential catalyst for chemical and biological reactions [42–44]. Because of the structural combination of TiO and the electron-rich porphyrin ligand, it is of interest to extend the theoretical study to the photo-assisted *de*N_2O. In this work, we theoretically investigated the reaction mechanism of *de*N_2O with the TiO-por catalyst by using density functional theory (DFT), and included a water molecule at the active site, and studied O_2 desorption as well.

2. Results and Discussion

The presence of water in the system might provide some steric hindrance around the active site and increase the activation energy barriers of the reaction. Hence, the effect of water was intensively studied in this work. Considering water molecule at the TiO site (Figure 1), we divided the N_2O decomposition over the TiO-por into four elementary steps as follows.

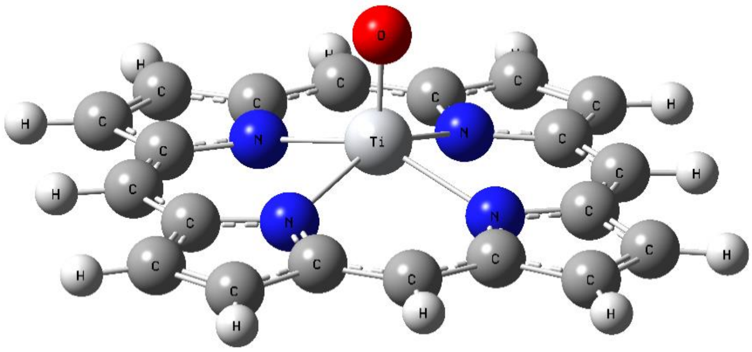

Figure 1. Structure of oxotitanium(IV) porphyrin (TiO-por).

Step 1: Water-complex formation on TiO-por

$$\text{TiO-por} + H_2O \rightarrow \text{Ti(OH)}_2\text{-por} \tag{2}$$

Step 2: First N_2O decomposition

$$\text{Ti(OH)}_2\text{-por} + \text{1st } N_2O \rightarrow \text{TiO(OH)}_2\text{-por} + N_2 \tag{3}$$

Step 3-A: Second N_2O decomposition followed by water desorption (Path A)

$$\text{TiO(OH)}_2\text{-por} + \text{2nd } N_2O \rightarrow \text{Ti(OOH)}_2\text{-por} + N \tag{4}$$

$$\text{Ti(OOH)}_2\text{-por} \rightarrow \text{TiO}_3\text{-por} + H_2O \tag{5}$$

Step 3-B: Water desorption followed by second N_2O decomposition (Path B)

$$\text{TiO(OH)}_2\text{-por} \rightarrow \text{TiO}_2\text{-por} + H_2O \tag{6}$$

$$\text{TiO}_2\text{-por} + \text{2nd } N_2O \rightarrow \text{TiO}_3\text{-por} + N_2 \tag{7}$$

Step 4: Catalyst regeneration; oxygen formation and desorption

$$\text{TiO}_3\text{-por} \rightarrow \text{TiO-por} + O_2 \tag{8}$$

As mentioned earlier, the thermal and photo-assisted reactions were simulated by using the DFT calculations of singlet and triplet states, respectively. The calculated activation energies of all steps in the singlet and triplet states are listed in Table 1. Based on the pairwise comparison, it can be clearly seen that in the overall reaction processes of N_2O direct decomposition in the photo-assisted condition, TiO-por (^{3}TiO-por) catalyst gives a more favorable reaction route with lower activation barriers. Therefore, the details of each reaction step in the photo-assisted condition will be further discussed. For the photo-absorption of the system, the absorption spectra of TiO-por and N_2O are compared in Figure S1. The first absorption band of TiO-por appears in the range of 300–400 nm which is assigned as the transition among the Gouterman's four orbitals (Figure S2). On the other hand, the absorption of N_2O appears at around 100–150 nm, in FUV region. Thus, the UV light irradiation selectively promotes TiO-por to the excited state which leads to the N_2O decomposition reaction. The spin density plot of the ^{3}TiO-por (Figure S3) also shows that the UV absorption is characterized as π–π* transition, with the spin density predominantly localized at meso-nitrogen positions.

Table 1. Activation energy (kcal/mol) for N_2O direct decomposition including the water molecule on singlet and triplet states of TiOH-por catalysts.

Reaction Step	Activation Energy (kcal/mol)	
	^{1}TiOH-por	^{3}TiOH-por
1st N_2O decomposition $Ti(OH)_2$-por + N_2O → $TiO(OH)_2$-por + N_2	63.57	27.57
Path A 2nd N_2O decomposition and water desorption $TiO(OH)_2$-por + N_2O → $Ti(OOH)_2$-por + N_2	67.87	29.01
Path B water desorption and 2nd N_2O decomposition TiO_2-por + N_2O → TiO_3-por + N_2	68.41	12.36
Oxygen formation TiO_3-por → TiO-por + O_2	5.12	*barrierless*

2.1. Water Dissociation over the TiO-por

The energy profile of water dissociation over the TiO-por is shown in Figure 2 with optimized structures. First, a water molecule approaches the TiO site, in which Ti is slightly above the porphyrin plane and this water molecule undergoes adsorption with the TiO-por (**AD1**), resulting in an energy change of −7.57 kcal/mol. The optimized **AD1** structure shows that a weak hydrogen bond is generated with a distance of 2.00 Å; the structural parameters of the adsorbed water are not significantly changed.

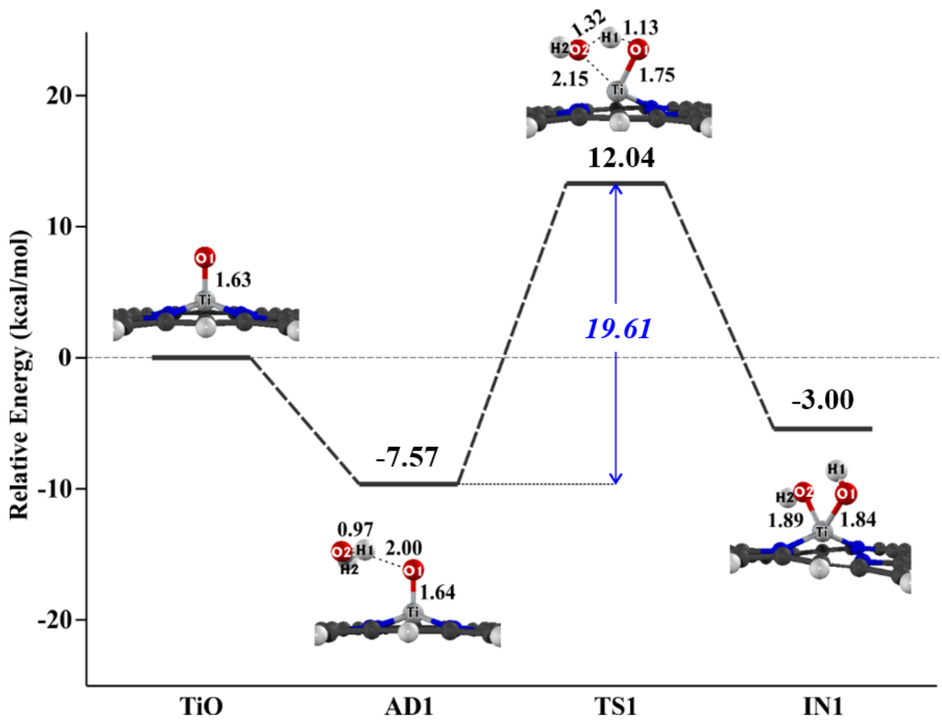

Figure 2. Water dissociation over the TiO-por active site. Light grey, red, blue, dark grey, and white balls represent Ti, O, N, C, and H atoms, respectively. Bond lengths are in Å.

The first step of the reaction is the concerted hydrogen transfer and Ti–O bond formation, which was preceded by the O2–H1 bond breaking and O1–H1 bond formation, as seen in the structure of **TS1**. The activation energy barrier of this step is 19.61 kcal/mol. The H1 of the water molecule forms a bond with the O1 with a distance of 1.13 Å and an <O1–H1–O2 angle of 138.5°. Because of this O–H bond formation, the Ti–O1 bond is elongated to 1.75 Å at an angle to the porphyrin plane. This structure results in the O2 atom of the water molecule being closer to the Ti atom. The imaginary frequency at **TS1** is 1284*i* cm^{-1}. The O1–H1 bond formation follows, with the O1–H1 bond distance of 0.96 Å. In addition, the Ti–O2 bond forms with a bond distance of 1.89 Å (**IN1**). Therefore, the new active site is generated as $Ti(OH)_2$ (**IN1**), from the water associated TiO-por catalyst. The relative energy of **IN1** is −3.00 kcal/mol, which is slightly exothermic, but endothermic when being relative to **AD1**.

2.2. First N_2O Decomposition

After water dissociation and formation of $Ti(OH)_2$ (**IN1**), the first N_2O decomposition proceeds. The reaction profile consists of four stationary points: N_2O adsorption, first transition state, N_2 production, and N_2 desorption, as displayed in Figure 3. The molecule weakly interacts with the OH via a hydrogen bond with an adsorption energy of −4.94 kcal/mol (**AD2**). Then, it forms a Ti–O3 bond (2.28 Å) at the transition state (**TS2**), in which the N_2O molecule shows a bent structure with an <O3–N1–N2 of 150°. The O3–N2 bond is elongated from 1.18 Å to 1.46 Å, indicating that the O3–N2 bond is activated. Because of this insertion, the Ti–O1 bond is elongated from 1.85 Å to 2.03 Å. This transition state has an activation energy barrier of 27.57 kcal/mol, with an imaginary frequency of 439*i* cm^{-1}. The N–O bond breaks at the next intermediate (**IN2**), and a Ti–O3 bond is formed with a distance of 1.93 Å. Because of this Ti–O3 bond formation, the Ti–O1 bond becomes weak and the O1 approaches the O3 atom with a distance of 1.45 Å. The product N_2 molecule is generated in this step. It requires 3.11 kcal/mol to desorb the N_2 molecule from the catalyst intermediate (**IN2-1**). Consequently, in the first N_2O decomposition step, the N_2O molecule weakly adsorbs over the hydroxyl-oxotitanium porphyrin ($Ti(OH)_2$-por) and the N_2O decomposition needs an activation energy of 27.57 kcal/mol to generate the N_2 molecule.

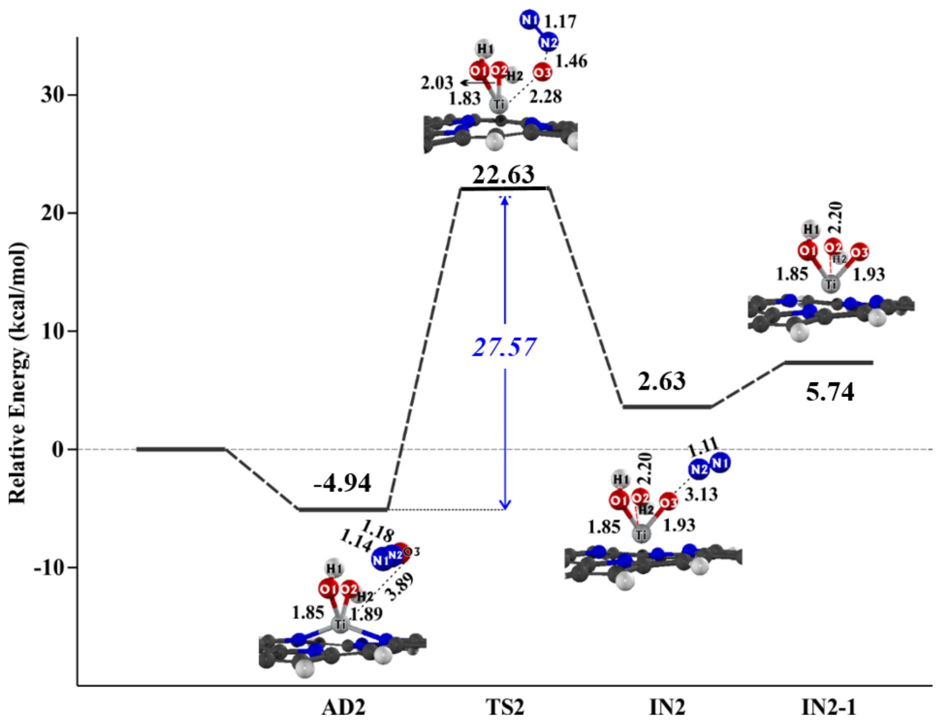

Figure 3. The first N_2O decomposition over the hydroxyl-oxotitanium porphyrin ($Ti(OH)_2$-por).

2.3. Second N_2O Decomposition

Two possible routes, Path A and Path B, were examined for the second N_2O decomposition. Path A is the case where the second N_2O is decomposed before water desorption. Alternatively, a water molecule is desorbed before the second N_2O decomposition in Path B.

Path A: The second N_2O decomposition (Figure 4) starts from the **IN2-1** ($TiO(OH)_2$-por) whose active site is coordinated by three oxygen atoms. All the steps of this decomposition proceed similarly to the first N_2O reaction. First, the **AD3A** intermediate is formed when a second N_2O is adsorbed on top of the **IN2-1**; the terminal O atom of N_2O interacts with the OH on the Ti center. The calculated adsorption energy is −3.77 kcal/mol. Through the transition state (**TS3$_A$**) at an imaginary frequency of 608*i* cm^{-1}, N–O bond dissociation occurs to form the intermediate **IN3$_A$** and a weakly interacting N_2 molecule. The activation energy barrier of this step is 29.01 kcal/mol, which is the same energy as the first N_2O decomposition. The produced N_2 desorbs from the active site, which requires 3.29 kcal/mol, and leaves the **IN3-1$_A$** intermediate, which consists of two OH groups coordinated at the Ti center. The resultant H_2O has a nearly linear structure with the <H1–O1–H2 angle being 171°. As a result, the H_2O molecule is formed easily (**IN4$_A$**) in an exothermic process, −20.34 kcal/mol relating to the **IN3-1$_A$** intermediate. Finally, the water molecule is generated and desorbed with energy of 9.61 kcal/mol (**IN4-1$_A$**).

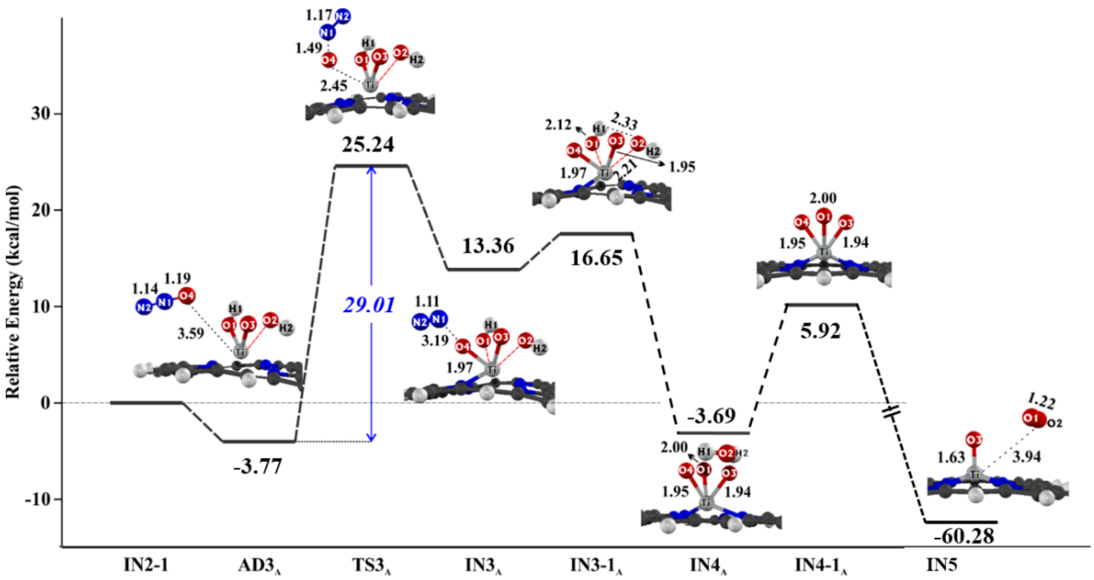

Figure 4. Path A: The second N_2O decomposition followed by water desorption and oxygen formation.

For Path B, when considering the structure of **IN2-1** (Figure 5) and the alternative pathway is also possible, namely, the H_2O molecule is released at the beginning, since the O1 has a hydrogen bond with the H2 atom and the distance is 2.25 Å with ∠H1–O1–H2 of about 171°. Thus, Path B starts from H_2O molecule desorption, which produces the intermediate **IN3$_B$**. The formation of the water molecule is an exothermic step with a relative energy of −11.59 kcal/mol. After the water desorption (**IN3-1$_B$**), the active site becomes the TiO_2-por intermediate. Then, the second N_2O interacts with the TiO_2-por intermediate with an energy change of −5.10 kcal/mol (**AD4$_B$**); this coordination is slightly stronger than the N_2O adsorption in Path A. To decompose the N_2O molecule over the TiO_2-por through the transition state (**TS4$_B$**) requires an activation energy of 12.37 kcal/mol, which is much lower than the case of Path A (**TS3$_A$**). This **TS4$_B$** has an imaginary frequency of 648*i* cm^{-1}, and the N_2O molecule has a bent structure with an ∠O3–N1–N2 angle of 126°. The O3 forms a Ti–O bond and the N1–O3 bond dissociates to give intermediate **IN4$_B$**. Finally, the N_2 molecule desorbs from **IN4$_B$**, which generates TiO_3-porphyrin (**IN4-1$_B$**). The calculated desorption energy of the N_2 molecule is 4.45 kcal/mol.

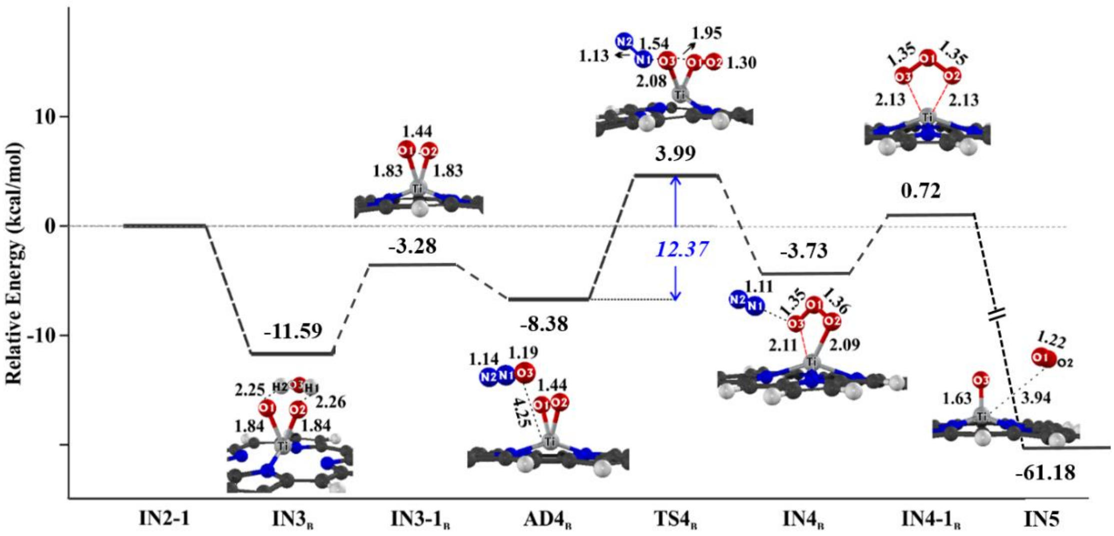

Figure 5. Path B: Water desorption followed by the second N_2O decomposition and oxygen formation.

In general, the rate-determining step of N_2O direct decomposition is desorption of the produced O_2 from the catalysts. The O_2 desorption from the active site usually requires high energy, which could prohibit reaction when the active site is deactivated [20,26,27,45,46]. However, our present work found that the O_2 is formed over the TiO_3 intermediate of **IN4-1$_A$** and **IN4-1$_B$** in both Path A and Path B, as shown in the last step of Figures 4 and 5, respectively. It is worth noting that O_2 molecule (**IN5** intermediate) is easily formed with activation energy of 6.45 kcal/mol and barrierless for Path A and Path B, respectively. Furthermore, this O_2 formation step is an extremely exothermic process. Therefore, it is shown that the TiO_3-por catalyst intermediate easily regenerates the active TiO-por catalyst, which is an advantage of this catalyst, compared with the related zeolite catalysts for N_2O decomposition [45,46].

2.4. Overall Energetics of Photo-Assisted N_2O Decomposition over Hydroxyl-Oxotitanium Porphyrin Catalysts

The overall reaction energy profile of the water dissociation followed by N_2O decomposition on the TiO-por is summarized in Figure 6. Initially, the water molecule is adsorbed on the TiO-por catalyst at −7.57 kcal/mol (**AD1**), and the active site becomes $Ti(OH)_2$ (**IN1**). As regarding to the first N_2O decomposition, the N_2O molecule is slightly adsorbed on $Ti(OH)_2$-por active site (**AD2**), requiring 27.57 kcal/mol (**TS2**) for the N–O dissociation to produce the N_2 molecule. The active site then becomes the $TiO(OH)_2$-por (**IN2-1**). Two pathways are possible starting from the **IN2-1** intermediate. In Path A, H_2O formation follows the second N_2O adsorption. The activation energy in this pathway is 29.01 kcal/mol (**TS3$_A$**). In Path B, the water molecule releases prior to N_2O decomposition. In Path B, the second N_2O decomposition occurs with an energy barrier of 12.37 kcal/mol (**TS4$_B$**). Therefore, the second N_2O decomposition over the TiO_2-por in Path B is expected to be more preferable than over the $TiO(OH)_2$-por of Path A, as summarized in Scheme 1. The final step is catalyst regeneration by oxygen molecule formation, and the calculated activation energy is barrierless to form the extremely exothermic intermediate, and the oxygen molecule easily desorbs from the surface of catalyst with only 4.96 kcal/mol. In the overall reaction, the N–O dissociation of the first N_2O molecule in Step 2 is the rate-determining step, which correlates well with the N_2O decomposition over Cu-ZSM5 [47]. It is worth to note that this present N_2O direct decomposition reaction has total reaction energy approximately at −52.58 kcal/mol.

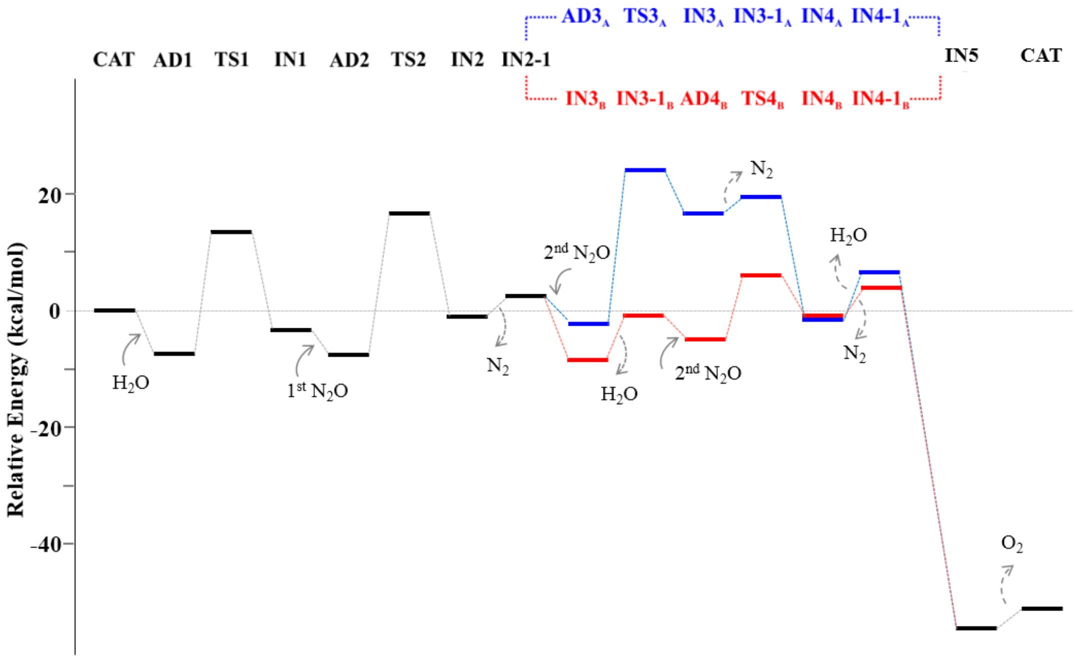

Figure 6. Full energy profile of N_2O decomposition over the oxotitanium porphyrin.

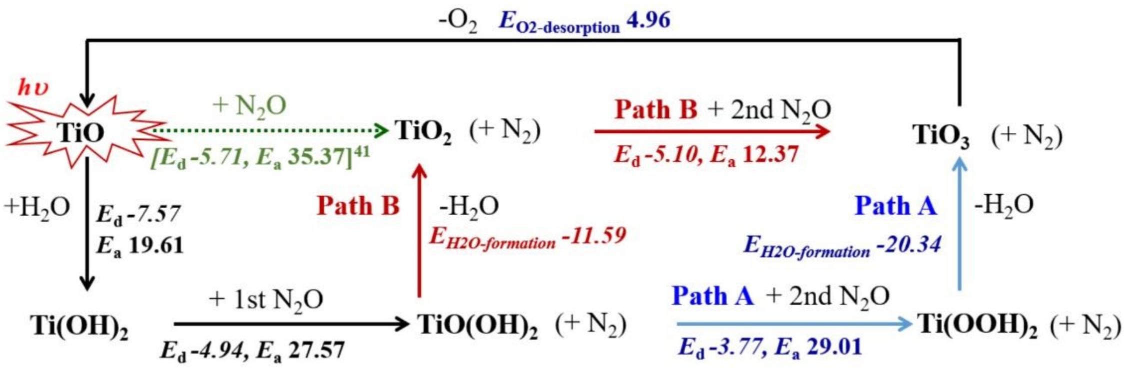

Scheme 1. Overall reaction pathways of the photo-assisted N_2O decomposition with/without a water molecule (the energy is in kcal/mol).

2.5. Effect of Water Molecule on the N_2O Decomposition Barriers

On the pairwise comparison of the theoretical reaction mechanism for N_2O decomposition with and without introducing H_2O, only a few works have addressed this issue [26,27]. It is well known that Fe-ZSM5 zeolite is one of the potential catalysts for N_2O direct decomposition and more importantly, theoretical analysis addressed the issue of activation barriers for the first and second N_2O decompositions and oxygen molecule formation. Thus, the present oxotitanium porphyrin catalyst for *de*N_2O with/without water molecule can be compared with the Fe-ZSM5 zeolite [27] to elucidate the catalytic potential and the effect of water. In Table 2, a comparison has been made between the Fe-ZSM5 zeolite catalysts with and without water in the N_2O decomposition, and these are represented by $Z^-[FeO]^+$ and $Z^-[Fe(OH)_2]^+$ active sites, respectively. It is clear that the $Z^-[Fe(OH)_2]^+$ active sites result in higher activation barriers to decompose the N_2O and form oxygen. Comparing oxotitanium porphyrin with and without water molecule represented by $^3Ti(OH)_2$-por and ^3TiO-por, [41] respectively, the N_2O decomposition over the $^3Ti(OH)_2$-por results in similar activation barriers as the ^3TiO-por active site [41]. In addition, these trends are also seen in the singlet state of oxotitanium porphyrin in this work. These results imply that the hydroxyl site of oxotitanium porphyrin produced by water dissociation does not increase the activation energy barrier for *de*N_2O, whereas the $Z^-[Fe(OH)_2]^+$ catalyst shows a significant increase in the activation energy barriers for the first and second N_2O decompositions and the desorption energy of the oxygen molecule.

Table 2. Activation energy (kcal/mol) of the first and second N_2O decompositions and oxygen formation over the Fe-ZSM5 and oxotitanium(IV) porphyrin.

Process	Activation Energy (kcal/mol)			
	$Z^-[FeO]^{+}$ [a]	**$Z^-[Fe(OH)_2]^{+}$ [a]**	**^{3}TiO-por [b]**	**$^3Ti(OH)_2$-por**
1st N_2O	30.4	42.8	29.9	27.6
2nd N_2O	20.1	61.7	11.5	12.4
O_2 formation	8.0	16.0	0.6	barrier less

[a] Ref [27], [b] Ref [41].

For the photo-assisted reaction, which is the main target in this work, the presence of water molecule on the active site of oxotitanium porphyrin has been intensively examined, to get a thorough view of the catalytic activity for N_2O decomposition, as displayed the overall reaction pathway in Scheme 1. In the absence of water [41], the first N_2O directly decomposes into N_2 product and $^3TiO_2$-por intermediate forms. The first N_2O adsorption on the TiO-por active site is −5.71 kcal/mol with activation energy barrier of 35.37 kcal/mol, it is worth mentioning that these energies do not include the zero-point energy (ZPE) correction [41]. In this reaction with presence of water, water molecule adsorption on the ^{3}TiO-por site (−7.57 kcal/mol) is stronger than the N_2O molecule. The water molecule more favorably covers the catalyst surface and generates the hydroxyl active site $^3Ti(OH)_2$-por. Over $^3Ti(OH)_2$-por active sites, the N_2O adsorption energy is −4.94 kcal/mol and the calculated energy barrier to decompose the N_2O is 27.57 kcal/mol. These results mean that the N_2O decomposition is not inhibited by the presence of water at the active site $^3Ti(OH)_2$-por. On the other hand, water molecules seem to act as an assisting reagent in the N_2O decomposition, as it can easily desorb after the N_2O decomposition process. Therefore, the TiO-por is proposed as a candidate catalyst for photo-assisted N_2O decomposition even under aqueous condition.

3. Computational Details

Nitrous oxide decomposition on the TiO-por model system was considered in the ground and excited states. The reaction pathways were calculated with the DFT method using the M06-L functional [48,49], in which full geometry optimization was performed without any geometrical restriction. To simulate the lowest lying excited state potential energy surface which represents the reaction under photo-irradiation, we adopted the unrestricted DFT (UM06L) method for triplet state calculation. The unrestricted DFT method is occasionally used for the calculations of photo-catalytic reactions [41,50,51]. The M06L functional has been examined with some variants of the coupled clusters [52,53] and other DFT functionals for systems including metals [52–54]. Although the energy barrier is sometimes underestimated, it works well in comparison with other global hybrid functionals. A basis set of double zeta plus polarization, i.e., 6-31G(d,p) was adopted for C, O, N, and H atoms, and the relativistic effective core potential of Hay–Wadt (LANL2DZ) was used for the Ti atom. All calculations were carried out with the Gaussian09 suite of programs Rev. B01 [55].

For the *de*NO_x simulation, H_2O and N_2O gases were used as the reactants. We considered both singlet and triplet spin states to simulate the reactions under thermal and photo-assisted conditions, respectively, the latter of which is assumed to be continuous photo-excitation with a considerable lifetime in the excited state without radiative or nonradiative decay. A vibrational analysis was done at each stationary point; all the intermediates were confirmed as true local minima and the transition states were first-order saddle points with only one imaginary frequency. The reaction energy profiles in terms of electronic with ZPE correction were calculated. The energy profile at each step was presented in the relative energy, which is defined as

$$\Delta E = E_{complex} - \left(E_{catalyst} + E_{adsorbate}\right) \quad (9)$$

where $E_{complex}$, $E_{catalyst}$, and $E_{adsorbate}$ are the total energies of the catalyst-adsorbate complex, the starting TiO-por complex at each step, and the isolated reactant molecules, respectively. The negative (positive) value indicates the stable (unstable) adsorption complex relative to the isolated systems.

4. Conclusions

The elementary reactions of N_2O decomposition over the oxotitanium porphyrin under thermal and photo-assisted conditions in the presence of water have been examined using DFT method with the unrestricted M06L/6-31G(d, p) level of theory. The potential energy profiles show that the entire reaction is an exothermic process. The reaction steps of N_2O decomposition over hydroxyl-oxotitanium porphyrin can be summarized as follows. For the first N_2O decomposition, the N–O bond dissociation over the $Ti(OH)_2$-por intermediate is the rate-determining step and requires an activation energy of 27.57 kcal/mol. Then, a spontaneous process of releasing the H_2O from the $TiO(OH)_2$-por catalyst intermediates is the preferable route, as examined in Path B, and the second N_2O decomposition over the TiO_2-por requires a lower activation energy of 12.37 kcal/mol than the first one. In the last step of catalyst regeneration, the O_2 formation from the TiO_3-por intermediate is a spontaneous process with a barrierless activation energy and a desorption energy of oxygen molecule only 4.96 kcal/mol, which is an advantage of this kind of catalyst.

Therefore, from this theoretical investigation, it is worth noting that the presence of water does not inhibit the N_2O decomposition on the catalyst surface. As a final note, the exhaust gas contains various compounds such as H_2O, O_2, N_xO_y, CO_2, and therefore, a theoretical study on the N_2O decomposition reaction needs to consider the effect of other gases in the reaction mechanism as well. The comprehensive study of overall reaction mechanism, which involves all effects, will be useful to guide experimental catalyst development for *de*N_2O applications.

Supplementary Materials: The following are available online at http://www.mdpi.com/2073-4344/10/2/157/s1, Absorption spectrum of TiO-Por and N_2O calculated by TD-M06L method, relevant MOs (a) HOMO-1, (b) HOMO, (c) LUMO, and (d) LUMO+1, of TiO-Por upon excitations, and the spin density plot of triplet state TiO-Por.

Author Contributions: P.M. (Conceptualization, Methodology, Data curation, Formal analysis, Writing—original draft and review), V.P. (Funding acquisition, Supervision), S.N. (Investigation, Methodology, Resources, Supervision, Review & editing) and L.S. (Funding acquisition, Supervision). All authors have read and agreed to the published version of the manuscript.

Funding: This research was partially funded by the NANOTEC, NSTDA, Ministry of Science and Technology, Thailand, through its program of Research Network NANOTEC and Thailand Research Fund (RSA6180080 and RTA6080005) and the Shanghai Municipal Science and Technology Commission of Professional and Technical Service Platform for Designing and Manufacturing of Advanced Composite Materials (16DZ2292100).

Acknowledgments: We thank Nanoscale Simulation Laboratory at National Nanotechnology Center (NANOTEC). P.M. would like to specially thank to Ehara for kindly discussion.

Conflicts of Interest: The authors declare no conflict of interest.

References

1. Ravishankara, A.R.; Daniel, J.S.; Portmann, R.W. Nitrous Oxide (N_2O): The Dominant Ozone-Depleting Substance Emitted in the 21st Century. *Science* **2009**, *326*, 123–125. [CrossRef] [PubMed]
2. Kapteijn, F.; Rodriguez-Mirasol, J.; Moulijn, J.A. Heterogeneous catalytic decomposition of nitrous oxide. *Appl. Catal. B Environ.* **1996**, *9*, 25–64. [CrossRef]
3. Konsolakis, M. Recent Advances on Nitrous Oxide (N_2O) Decomposition over Non-Noble-Metal Oxide Catalysts: Catalytic Performance, Mechanistic Considerations, and Surface Chemistry Aspects. *ACS Catal.* **2015**, *5*, 6397–6421. [CrossRef]

4. Liu, Z.; He, F.; Ma, L.; Peng, S. Recent Advances in Catalytic Decomposition of N_2O on Noble Metal and Metal Oxide Catalysts. *Catal. Surv. Asia* **2016**, *20*, 121–132. [CrossRef]
5. Leont'ev, A.V.; Fomicheva, O.A.; Proskurnina, M.V.; Zefirov, N.S. Modern chemistry of nitrous oxide. *Russ. Chem. Rev.* **2001**, *70*, 91–104. [CrossRef]
6. Doi, K.; Noda, T.; Arai, T.L.N.; Tagawa, T.; Goto, S. Effects of Isoflurane on Kinetics of N_2O Catalytic Decomposition over Rh/Al_2O_3 in Medical Operating Rooms. *J. Chem. Eng. Jpn.* **2003**, *36*, 322–327. [CrossRef]
7. Doi, K.; Wu, Y.Y.; Takeda, R.; Matsunami, A.; Arai, N.; Tagawa, T.; Goto, S. Catalytic decomposition of N_2O in medical operating rooms over Rh/Al_2O_3, Pd/Al_2O_3, and Pt/Al_2O_3. *Appl. Catal. B Environ.* **2001**, *35*, 43–51. [CrossRef]
8. Wei, X.; Yang, X.-F.; Wang, A.-Q.; Li, L.; Liu, X.-Y.; Zhang, T.; Mou, C.-Y.; Li, J. Bimetallic Au–Pd Alloy Catalysts for N_2O Decomposition: Effects of Surface Structures on Catalytic Activity. *J. Phys. Chem. C* **2012**, *116*, 6222–6232. [CrossRef]
9. Hermes, A.C.; Hamilton, S.M.; Hopkins, W.S.; Harding, D.J.; Kerpal, C.; Meijer, G.; Fielicke, A.; Mackenzie, S.R. Effects of Coadsorbed Oxygen on the Infrared Driven Decomposition of N_2O on Isolated Rh_5^+ Clusters. *J. Phys. Chem. Lett.* **2011**, *2*, 3053–3057. [CrossRef]
10. Rodríguez-Kessler, P.L.; Rodríguez-Domínguez, A.R. N_2O dissociation on small Rh clusters: A density functional study. *Comput. Mater. Sci.* **2015**, *97*, 32–35. [CrossRef]
11. Rodríguez-Kessler, P.L.; Pan, S.; Florez, E.; Cabellos, J.L.; Merino, G. Structural Evolution of the Rhodium-Doped Silver Clusters AgnRh ($n \leq 15$) and Their Reactivity toward NO. *J. Phys. Chem. C* **2017**, *121*, 19420–19427. [CrossRef]
12. Russo, N.; Mescia, D.; Fino, D.; Saracco, G.; Specchia, V. N_2O Decomposition over Perovskite Catalysts. *Ind. Eng. Chem. Res.* **2007**, *46*, 4226–4231. [CrossRef]
13. Jiang, H.; Wang, H.; Liang, F.; Werth, S.; Schiestel, T.; Caro, J. Direct Decomposition of Nitrous Oxide to Nitrogen by In Situ Oxygen Removal with a Perovskite Membrane. *Angew. Chem. Int. Ed.* **2009**, *48*, 2983–2986. [CrossRef] [PubMed]
14. Sui, C.; Niu, X.; Wang, Z.; Yuan, F.; Zhu, Y. Activity and deactivation of Ru supported on $La_{1.6}Sr_{0.4}NiO_4$ perovskite-like catalysts prepared by different methods for decomposition of N_2O. *Catal. Sci. Technol.* **2016**, *6*, 8505–8515. [CrossRef]
15. Liu, N.; Chen, P.; Li, Y.; Zhang, R. N_2O Direct Dissociation over $Mg_xCe_yCo_{1-x-y}Co_2O_4$ Composite Spinel Metal Oxide. *Catalysts* **2017**, *7*, 10. [CrossRef]
16. Kaczmarczyk, J.; Zasada, F.; Janas, J.; Indyka, P.; Piskorz, W.; Kotarba, A.; Sojka, Z. Thermodynamic Stability, Redox Properties, and Reactivity of Mn_3O_4, Fe_3O_4, and Co_3O_4 Model Catalysts for N_2O Decomposition: Resolving the Origins of Steady Turnover. *ACS Catal.* **2016**, *6*, 1235–1246. [CrossRef]
17. Abu-Zied, B.M.; Bawaked, S.M.; Kosa, S.A.; Ali, T.T.; Schwieger, W.; Aqlan, F.M. Effects of Nd-, Pr-, Tb- and Y-doping on the structural, textural, electrical and N_2O decomposition activity of mesoporous NiO nanoparticles. *Appl. Surf. Sci.* **2017**, *419*, 399–408. [CrossRef]
18. Carabineiro, S.A.C.; Papista, E.; Marnellos, G.E.; Tavares, P.B.; Maldonado-Hódar, F.J.; Konsolakis, M. Catalytic decomposition of N_2O on inorganic oxides: Effect of doping with Au nanoparticles. *Mol. Catal.* **2017**, *436*, 78–89. [CrossRef]
19. Kondratenko, E.V.; Pérez-Ramírez, J. Mechanism and Kinetics of Direct N_2O Decomposition over Fe−MFI Zeolites with Different Iron Speciation from Temporal Analysis of Products. *J. Phys. Chem. B* **2006**, *110*, 22586–22595. [CrossRef]
20. Liu, N.; Zhang, R.; Chen, B.; Li, Y.; Li, Y. Comparative study on the direct decomposition of nitrous oxide over M (Fe, Co, Cu)–BEA zeolites. *J. Catal.* **2012**, *294*, 99–112. [CrossRef]
21. Uzunova, E.L.; Mikosch, H. A theoretical study of nitric oxide adsorption and dissociation on copper-exchanged zeolites SSZ-13 and SAPO-34: The impact of framework acid-base properties. *Phys. Chem. Chem. Phys.* **2016**, *18*, 11233–11242. [CrossRef] [PubMed]
22. Guesmi, H.; Berthomieu, D.; Bromley, B.; Coq, B.; Kiwi-Minsker, L. Theoretical evidence of the observed kinetic order dependence on temperature during the N_2O decomposition over Fe-ZSM-5. *Phys. Chem. Chem. Phys.* **2010**, *12*, 2873–2878. [CrossRef] [PubMed]
23. Marnellos, G.E.; Efthimiadis, E.A.; Vasalos, I.A. Effect of SO_2 and H_2O on the N_2O decomposition in the presence of O_2 over Ru/Al_2O_3. *Appl. Catal. B Environ.* **2003**, *46*, 523–539. [CrossRef]

24. Marnellos, G.E.; Efthimiadis, E.A.; Vasalos, I.A. Simultaneous Catalytic Reduction of NO_X and N_2O in an $In/Al_2O_3-Ru/Al_2O_3$ Dual-Bed Reactor in the Presence of SO_2 and H_2O. *Ind. Eng. Chem. Res.* **2004**, *43*, 2413–2419. [CrossRef]
25. Hansen, N.; Heyden, A.; Bell, A.T.; Keil, F.J. A Reaction Mechanism for the Nitrous Oxide Decomposition on Binuclear Oxygen Bridged Iron Sites in Fe-ZSM-5. *J. Phys. Chem. C* **2007**, *111*, 2092–2101. [CrossRef]
26. Heyden, A.; Hansen, N.; Bell, A.T.; Keil, F.J. Nitrous Oxide Decomposition over Fe-ZSM-5 in the Presence of Nitric Oxide: A Comprehensive DFT Study. *J. Phys. Chem. B* **2006**, *110*, 17096–17114. [CrossRef]
27. Heyden, A.; Peters, B.; Bell, A.T.; Keil, F.J. Comprehensive DFT Study of Nitrous Oxide Decomposition over Fe-ZSM-5. *J. Phys. Chem. B* **2005**, *109*, 1857–1873. [CrossRef]
28. Bulushev, D.A.; Prechtl, P.M.; Renken, A.; Kiwi-Minsker, L. Water Vapor Effects in N_2O Decomposition over Fe−ZSM-5 Catalysts with Low Iron Content. *Ind. Eng. Chem. Res.* **2007**, *46*, 4178–4185. [CrossRef]
29. Ju, W.-S.; Matsuoka, M.; Iino, K.; Yamashita, H.; Anpo, M. The Local Structures of Silver(I) Ion Catalysts Anchored within Zeolite Cavities and Their Photocatalytic Reactivities for the Elimination of N_2O into N_2 and O_2. *J. Phys. Chem. B* **2004**, *108*, 2128–2133. [CrossRef]
30. Schneider, J.; Matsuoka, M.; Takeuchi, M.; Zhang, J.; Horiuchi, Y.; Anpo, M.; Bahnemann, D.W. Understanding TiO_2 Photocatalysis: Mechanisms and Materials. *Chem. Rev.* **2014**, *114*, 9919–9986. [CrossRef]
31. Higashimoto, S.; Nishimoto, K.; Ono, T.; Anpo, M. Characterization of Fe-Oxide Species Prepared onto ZSM-5 Zeolites and Their Role in the Photocatalytic Decomposition of N_2O into N_2 and O_2. *Chem. Lett.* **2000**, *29*, 1160–1161. [CrossRef]
32. Rusu, C.N.; Yates, J.T. N_2O Adsorption and Photochemistry on High Area TiO_2 Powder. *J. Phys. Chem. B* **2001**, *105*, 2596–2603. [CrossRef]
33. Sano, T.; Negishi, N.; Mas, D.; Takeuchi, K. Photocatalytic Decomposition of N_2O on Highly Dispersed Ag^+ Ions on TiO_2 Prepared by Photodeposition. *J. Catal.* **2000**, *194*, 71–79. [CrossRef]
34. Kim, B.; Li, Z.; Kay, B.D.; Dohnálek, Z.; Kim, Y.K. Low-Temperature Desorption of N_2O from NO on Rutile $TiO_2(110)$-1 × 1. *J. Phys. Chem. C* **2014**, *118*, 9544–9550. [CrossRef]
35. Obalová, L.; Reli, M.; Lang, J.; Matějka, V.; Kukutschová, J.; Lacný, Z.; Kočí, K. Photocatalytic decomposition of nitrous oxide using TiO_2 and Ag-TiO_2 nanocomposite thin films. *Catal. Today* **2013**, *209*, 170–175. [CrossRef]
36. Kočí, K.; Krejčíková, S.; Šolcová, O.; Obalová, L. Photocatalytic decomposition of N_2O on Ag-TiO_2. *Catal. Today* **2012**, *191*, 134–137. [CrossRef]
37. Chatterjee, T.; Shetti, V.S.; Sharma, R.; Ravikanth, M. Heteroatom-Containing Porphyrin Analogues. *Chem. Rev.* **2017**, *117*, 3254–3328. [CrossRef]
38. Zhang, W.; Lai, W.; Cao, R. Energy-Related Small Molecule Activation Reactions: Oxygen Reduction and Hydrogen and Oxygen Evolution Reactions Catalyzed by Porphyrin- and Corrole-Based Systems. *Chem. Rev.* **2017**, *117*, 3717–3797. [CrossRef]
39. Gao, W.-Y.; Chrzanowski, M.; Ma, S. Metal-metalloporphyrin frameworks: A resurging class of functional materials. *Chem. Soc. Rev.* **2014**, *43*, 5841–5866. [CrossRef]
40. Antonangelo, A.R.; Grazia Bezzu, C.; Mughal, S.S.; Malewschik, T.; McKeown, N.B.; Nakagaki, S. A porphyrin-based microporous network polymer that acts as an efficient catalyst for cyclooctene and cyclohexane oxidation under mild conditions. *Catal. Commun.* **2017**, *99*, 100–104. [CrossRef]
41. Maitarad, P.; Namuangruk, S.; Zhang, D.; Shi, L.; Li, H.; Huang, L.; Boekfa, B.; Ehara, M. Metal–Porphyrin: A Potential Catalyst for Direct Decomposition of N_2O by Theoretical Reaction Mechanism Investigation. *Environ. Sci. Technol.* **2014**, *48*, 7101–7110. [CrossRef] [PubMed]
42. Guilard, R.; Latour, J.M.; Lecomte, C.; Marchon, J.C.; Protas, J.; Ripoll, D. Peroxotitanium (IV) porphyrins. Synthesis, stereochemistry, and properties. *Inorg. Chem.* **1978**, *17*, 1228–1237. [CrossRef]
43. Woo, L.K.; Hays, J.A.; Goll, J.G. Oxo-transfer reactions of chromium and titanium porphyrins. *Inorg. Chem.* **1990**, *29*, 3916–3917. [CrossRef]
44. Latour, J.-M.; Galland, B.; Marchon, J.-C. Retention of configuration at the titanium atom upon oxo-peroxo ligand substitution of titanium (IV) porphyrins. *J. Chem. Soc. Chem. Commun.* **1979**, *13*, 570–571. [CrossRef]
45. Pirngruber, G.D. The surface chemistry of N_2O decomposition on iron containing zeolites (I). *J. Catal.* **2003**, *219*, 456–463. [CrossRef]
46. Winter, E.R.S. The decomposition of nitrous oxide on the rare-earth sesquioxides and related oxides. *J. Catal.* **1969**, *15*, 144–152. [CrossRef]

47. Liu, X.; Yang, Z.; Zhang, R.; Li, Q.; Li, Y. Density Functional Theory Study of Mechanism of N_2O Decomposition over Cu-ZSM-5 Zeolites. *J. Phys. Chem. C* **2012**, *116*, 20262–20268. [CrossRef]
48. Zhao, Y.; Truhlar, D.G. The M06 suite of density functionals for main group thermochemistry, thermochemical kinetics, noncovalent interactions, excited states, and transition elements: Two new functionals and systematic testing of four M06-class functionals and 12 other functionals. *Theor. Chem. Acc.* **2008**, *120*, 215–241.
49. Zhao, Y.; Truhlar, D.G. Density Functional Theory for Reaction Energies: Test of Meta and Hybrid Meta Functionals, Range-Separated Functionals, and Other High-Performance Functionals. *J. Chem. Theory Comput.* **2011**, *7*, 669–676. [CrossRef]
50. Mom, R.V.; Cheng, J.; Koper, M.T.M.; Sprik, M. Modeling the Oxygen Evolution Reaction on Metal Oxides: The Infuence of Unrestricted DFT Calculations. *J. Phys. Chem. C* **2014**, *118*, 4095–4102. [CrossRef]
51. Enriquez, J.I.G.; Moreno, J.L.V.; David, M.Y.; Arboleda, N.B.; Lin, O.H.; Villagracia, A.R.C. DFT Investigation on the Electronic and Water Adsorption Properties of Pristine and N-Doped TiO_2 Nanotubes for Photocatalytic Water Splitting Applications. *J. Electron. Mater.* **2017**, *46*, 3592–3602. [CrossRef]
52. Hansen, J.A.; Ehara, M.; Piecuch, P. Aerobic Oxidation of Methanol to Formic Acid on Au_8^-: Benchmark Analysis Based on Completely Renormalized Coupled-Cluster and Density Functional Theory Calculations. *J. Phys. Chem. A* **2013**, *117*, 10416–10427. [CrossRef] [PubMed]
53. Boekfa, B.; Pahl, E.; Gaston, N.; Sakurai, H.; Limtrakul, J.; Ehara, M. C–Cl Bond Activation on Au/Pd Bimetallic Nanocatalysts Studied by Density Functional Theory and Genetic Algorithm Calculations. *J. Phys. Chem. C* **2014**, *118*, 22188–22196. [CrossRef]
54. Meeprasert, J.; Namuangruk, S.; Boekfa, B.; Dhital, R.N.; Sakurai, H.; Ehara, M. Mechanism of Ullmann Coupling Reaction of Chloroarene on Au/Pd Alloy Nanocluster: A DFT Study. *Organometallics* **2016**, *35*, 1192–1201. [CrossRef]
55. Frisch, M.J.; Trucks, G.W.; Schlegel, H.B.; Scuseria, G.E.; Robb, M.A.; Cheeseman, J.R.; Scalmani, G.; Barone, V.; Petersson, G.A.; Nakatsuji, H.; et al. *Gaussian 09 Rev. B.01*; Gaussian Inc.: Wallingford, CT, USA, 2010.